ACS OMEGA

Article

Cite This: ACS Omega 2019, 4, 535−545

http://pubs.acs.org/journal/acsodf

Ultrasonic Synthesis of Carbon Nanotube-Titanium Dioxide Composites: Process Optimization via Response Surface Methodology

Qammer Zaib,[†,‡] Mustapha Jouiad,[§,∥] and Farrukh Ahmad*[,†]

[†]Department of Civil, Infrastructure and Environmental Engineering and [§]Materials Science & Engineering, Khalifa University of Science and Technology, Masdar City Campus, P.O. Box 54224, Abu Dhabi, UAE

[‡]Department of Civil and Environmental Engineering, University of Ulsan, 93 Daehakro, Ulsan 680-749, South Korea

Supporting Information

ABSTRACT: In this study, the central composite design of response surface methodology was applied to optimize the ultrasonic synthesis of multiwalled carbon nanotube-titanium dioxide (MWNT-TiO_2) composites. Twenty composites were prepared by adjusting three parameters (MWNT concentration in water, sonication to disperse/exfoliate MWNTs in water, and sonication to attach TiO_2 onto MWNTs) at five levels. On the basis of the experimental design, semiempirical expressions were developed, analyzed, statistically assessed, and subsequently applied to predict the impact of the studied parameters on composite synthesis. The composite synthesis process was optimized to capture the experimental conditions favoring the highest productivity (i.e., MWNT-TiO_2 formation or percent TiO_2 attachment) utilizing minimal resources. The synthesis process optimization results showed that, to make a MWNT-TiO_2 composite in 10 mL of water, 23.2 mg (~99% of 23.4 mg) of TiO_2 can be attached to 2.6 mg of MWNTs. This process requires only 727 J sonication energy, of which 592 J is invested to exfoliate MWNTs (Sonication 1) and 135 J to attach TiO_2 (Sonication 2) to MWNTs. Finally, the optimally synthesized composite was extensively characterized using SEM, surface area and porosity analysis, TGA, and ζ-potential analysis/DLS. Also, this composite was tested for stability under variable pH and solvent polarity. The approach developed in this study could be used to optimize the synthesis process of other similar composites.

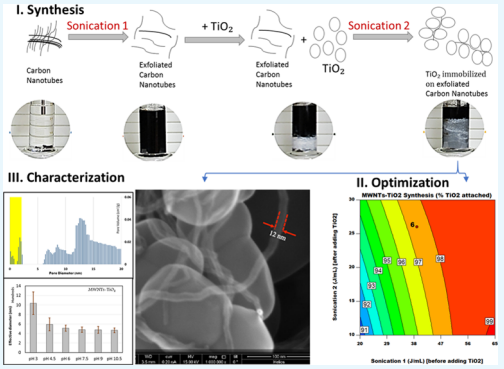

1. INTRODUCTION

The photocatalytic activity of TiO_2 has been extensively studied for removing organic pollutants from air and water.[1−12] In water treatment experiments, TiO_2 particles are often used as suspensions in a batch slurry photoreactor.[13,14] The slurry reactors are efficient at photocatalytic performance but carry some economic and practical limitations. One of the big problems of using TiO_2 in slurry form is its recovery after treatment so that it can be reused. The TiO_2 crystalline particles are usually nonporous; therefore, their size is reduced to maximize their surface area for enhanced performance. This small size carries with it the penalty of high filtration costs.[15,16] Also, the performance of inner TiO_2 particles (floating deep inside the suspension) is adversely affected by outer surrounding particles. Inner particles receive limited light to photo-activate[17,18] because most of the light, including short-wavelength UV, is absorbed by outer surrounding particles. Lastly, reports about the TiO_2 toxicity in the recent literature have prompted calls for its complete removal from the ecosystem.[18] These issues have led to the development of supported photocatalysts in recent years.[17,19,20] The most desirable characteristics of photocatalysis support materials include (i) enhancement of TiO_2 photocatalysis, (ii) high surface area to accommodate maximum attachment of TiO_2, and (iii) robustness to resist reactive species generated during photocatalysis.

The first common choice is finding the support for anatase TiO_2 in its other crystalline forms. Anatase is selected for this study because of its superior photoactivity performance among the polymorphs of TiO_2.[10,21,22] Rutile phase TiO_2 can be thermally attached to an inert substrate (glass) and used as a support because it is the most stable crystalline form (i.e., strong enough to resist reactive species) and because it enhances the photocatalytic activity of anatase. The literature reports an increased photoreactivity of mixed phase TiO_2 compared to a pure phase one.[2−8] This enhancement is believed to be due to a spatial separation at the solid−solid interfaces, leading to reduced electron−hole recombination.[3−8] In the case of commercial Degussa P25 (usually 0.8:0.2 = anatase/rutile mixture), the rutile acts as an electron sink,[3,4,23] thereby delaying

Received: October 8, 2018
Accepted: December 20, 2018
Published: January 8, 2019

DOI: 10.1021/acsomega.8b02706
ACS Omega 2019, 4, 535−545

electron−hole recombination. The enhancement in the photocatalytic activity of anatase and its robustness against photoreactive species make rutile an eligible candidate as a support material; however, it lacks a high surface area. Usually, the surface area of rutile is equal to or less than that of anatase.[21,24]

Surface area limitations were resolved by replacing rutile TiO_2 with activated carbon, which is well known for its high surface area.[25] Activated carbon was also found to effectively enhance the photoreactivity of anatase.[20,26−28] A few reports in the literature suggested activated carbon's superiority in enhancing the photocatalytic activity of anatase compared to rutile (in Degussa P25).[29,30] Therefore, activated carbon can be used as a support material owing to its role in enhancing the photocatalytic activity of anatase and because of its high surface area;[20,26−30] however, its amorphous structure is prone to degradation by photoreactive species. Additionally, most of the surface area of activated carbon is due to its micropores, sites that are unsuitable for anchoring TiO_2 because of the unavailability of light in such narrow internal spaces.[25]

In this study, carbon nanotubes (CNTs) were used to immobilize TiO_2. CNTs are known to enhance its photocatalytic activity by delaying electron−hole recombination.[6,23,31−38] More specifically, the immobilization of TiO_2 onto multiwalled carbon nanotubes (MWNTs) was carried out with the aid of ultrasonication (aka sonication). MWNTs were exfoliated by sonication in aqueous media to allow TiO_2 particles to attach to their surface. The influence of operational sonication parameters on the exfoliation of MWNTs and subsequent attachment of TiO_2 was studied by response surface methodology (RSM). RSM helps in determining the quantitative relationship between controllable input parameters (variables or factors) and their contribution to a desired response. Hence, it optimizes the response surface with respect to process parameters.[39,40] RSM requires the following design procedures:[17,41] (i) a series of experiments to measure desired response adequately and reliably; (ii) development of a best fit mathematical model for a second-order response surface; (iii) determination of experimental parameters that are most sensitive to the response; and (iv) the representation of individual and interactive effects of factors on responses. RSM can help in estimating the linear, interaction, and quadratic effects of the factors and yields a prediction model for responses. Therefore, it can be used to identify the optimal process settings for achieving the efficient use of resources. The two most common designs used in RSM are the Box−Behnken design (BBD) and the central composite design (CCD).[42−44] BBD is a three-level design, whereas CCD is a five-level fractional factorial design that constructs the second-order response surface. CCD is more frequently used because it gives almost as much information as provided by multilevel factorial design. However, it requires far fewer experiments than a full factorial design.[45−47]

Several researchers have used sonication for attaching metal oxide particles to carbonaceous materials.[6] However, to the best of our knowledge, no optimization study using RSM has been performed to identify and quantify the role of sonication on the formation of metal oxide-carbonaceous material composites. In this study, RSM was applied to optimize TiO_2 attachment onto MWNTs to synthesize MWNT-TiO_2 composites. The factors investigated were (i) the concentration of MWNTs in water, (ii) sonication to exfoliate MWNTs, and (iii) sonication to keep MWNTs exfoliated and provide mixing to facilitate the attachment of TiO_2 on their surfaces. The responses studied were (i) expansion of MWNT bed volume in water and (ii) percent attachment of TiO_2 on MWNTs. A model was developed, statistically tested, and experimentally validated to represent the effect of factors on responses. Also, the operational parameters were optimized to maximize the TiO_2 attachment at minimum resource expenditure. Finally, the product (MWNT-TiO_2 composite) prepared from the optimized procedure and its constituent materials (MWNTs and TiO_2) were characterized using electron microscopy, surface area and porosity analyses, TGA, and ζ-potential analysis. Also, the composite was tested for its structural integrity in extreme environments, such as highly acidic/basic and polar/nonpolar media.

2. MATERIALS AND METHODS

2.1. Materials. *2.1.1. Chemicals and Reagents.* MWNTs, prepared by catalytic carbon vapor deposition method having an average diameter of 10−12 nm, and other chemicals, such as titanium dioxide (anatase), potassium phosphate, hydrochloric acid, and sodium chloride, were purchased from Sigma-Aldrich (St. Louis, MO, USA). Fresh deionized water with an average resistivity of 18.2 MΩ·cm was used throughout the course of experimentation.

2.1.2. Sonication and Filtration. Sonication was performed using Q125 (QSonica LLC, Newton, CT, USA) with preoptimized sonicator operating parameters for MWNT dispersion (amplitude = 145 μm and pulse on/off cycle = 45/30 s). Vacuum filtration was carried out on glass microfiber filters (GF/F) with an average pore size of 700 nm using Millipore apparatus (Millipore Corp., Billerica, MA, USA).

2.2. CCD for Synthesis and Optimization of MWNT-TiO_2 Composite. Synthesis of MWNT-TiO_2 composite was a four-step process: (i) addition of MWNTs to deionized water, (ii) Sonication 1, to disperse/exfoliate MWNTs, (iii) addition of TiO_2, and (iv) Sonication 2, for mixing and further exfoliation of MWNTs and to attach TiO_2 onto MWNT surface. The mass of TiO_2 in step three was kept proportionally constant to the mass of MWNTs in step one. The MWNT:TiO_2 mass ratio was 1:9 in all studied systems because MWNT-TiO_2 composites failed to form a film at higher concentrations of TiO_2: a critical characteristic required for surface coating and membrane synthesis applications (Figure S1 in the Supporting Information). Therefore, the first, second, and fourth steps (variables or factors) were analyzed and optimized by RSM, a chemometric approach. CCD was developed to establish the relationship between synthesis variables (factors) and product characteristics (responses): (i) expansion/exfoliation of MWNTs and (ii) attachment of TiO_2 to MWNTs.

The process of synthesis and optimization of MWNT-TiO_2 composite was divided into eight steps as described below:

1. Variables were evaluated to estimate their correlation to responses. This helped in estimating the relative importance of variables.
2. A model was developed to describe and predict the influence of variables on responses.
3. The model was tested for its effectiveness in predicting the responses.
4. Statistical analyses were performed on the model to establish its validity. Analysis of variance (ANOVA) of the model and its terms was carried out for this purpose.
5. The contribution of the individual variables and the combined effects of variables on responses were quantified. For this purpose, perturbation and Pareto plots were generated.

DOI: 10.1021/acsomega.8b02706
ACS Omega 2019, 4, 535−545

Table 1. Variables and Levels of Chosen Factors for CCD

			coded levels				
factor	variable	unit	$-\alpha$	−1	0	1	α
A	MWNT conc.	mg/mL	0.082	0.13	0.2	0.27	0.31
B	Sonication 1	J/mL	5	18	39	59	73
C	Sonication 2	J/mL	5	13	26	39	47

Table 2. Experimental Design Matrix Based on a CCD Using Full Factorial

		input variables (factors)			MWNT expansion (1000× expanded)			TiO_2 attachment (% attached)		
run	space type	*A*: MWNT conc. (mg/mL)	*B*: Sonication 1 (J/mL)	*C*: Sonication 2 (J/mL)	experimental	predicted	% error	experimental	predicted	% error
1	factorial	0.13	59	14	15.8	13.5	14.1	97.5	98.8	1.4
2	factorial	0.27	19	14	3.5	3.9	8.7	90.9	90.7	0.3
3	center	0.20	39	26	10.5	10.5	0.1	96.8	97.6	0.9
4	factorial	0.13	59	38	15.8	17.1	8.7	98.1	98.0	0.2
5	factorial	0.27	59	14	9.8	10.1	2.7	98.0	99.3	1.3
6	factorial	0.13	19	14	7.9	7.3	7.7	91.4	90.2	1.3
7	center	0.20	39	26	10.5	10.5	0.1	97.9	97.6	0.3
8	factorial	0.13	19	38	11.8	10.9	8.0	97.1	95.8	1.4
9	factorial	0.27	59	38	11.8	13.7	16.1	98.4	98.4	0.0
10	center	0.20	39	26	10.5	10.5	0.1	99.0	97.6	1.4
11	axial	0.20	39	47	13.1	13.5	3.0	98.1	99.6	1.5
12	axial	0.20	73	26	15.8	15.8	0.0	99.3	97.5	1.8
13	center	0.20	39	26	10.5	10.5	0.1	97.6	97.6	0.0
14	center	0.20	39	26	10.5	10.5	0.1	97.8	97.6	0.2
15	axial	0.20	5	26	4.2	5.2	24.4	86.8	88.4	1.8
16	axial	0.08	39	26	12.1	13.4	10.5	95.7	97.2	1.5
17	axial	0.20	39	5	5.3	7.5	42.1	95.9	95.6	0.3
18	axial	0.32	39	26	8.4	7.6	9.4	97.8	98.0	0.2
19	factorial	0.27	19	38	7.9	7.5	5.4	97.2	96.3	0.9
20	center	0.20	39	26	10.5	10.5	0.1	97.7	97.6	0.1

6. Optimization criteria were developed.
7. The optimized range of variables and their effects on desirable responses were identified.
8. Finally, contours were developed to exhibit the optimized region for the desired responses.

Design-Expert 9.0.6 software (Stat-Ease, Inc., MN, USA) was used for experimental design and the analysis of experimental data. Table 1 summarizes the ranges and levels of the studied variables. The three factors were converted to dimensionless variables (*A*, *B*, and *C*) with coded values at five levels. The dimensionless variables were obtained by subtracting the actual value of variable from its value at the central point and dividing it by the step chance value because regression analysis could not be performed on raw physical (dimensional) parameters. Coding was performed to normalize the parameters because each coded variable is forced to range from $-\alpha$ to $+\alpha$ (explained herein) so that it affects the response evenly. The numerical ranges of variables were determined by preliminary experiments. Figure S2 shows the rotatable CCD experimental points and design space that were followed in this study. CCD consists of three types of points: factorial, axial, and central. The central point is often used to calculate the experimental error. The distance of an axial point from the center is denoted by α, and it depends on a number of factors chosen for the design. The CCD approach reduced the number of experiments from 5^3 =125, which were otherwise required for full factorial design, to only 20. Accordingly, a total of 20 experiments were performed to determine 8 factorial, 6 axial, and 6 center points. The complete array of experiments and the exact experimental conditions of factorial, central, and axial points of CCD can be seen in Table 2.

2.3. MWNT Expansion and TiO_2 Attachment. The dispersion of MWNTs was determined by a semiquantitative technique. A stable (up to 24 h) expansion in bed volume of MWNTs after sonication was considered proportional to its exfoliation. A specific mass of MWNTs was allowed to expand during sonication. The volume occupied by an expanded bed of MWNTs, hence obtained after sonication, was divided by its initial bed volume. It was observed that, in the studied sonication range, the bed volume of MWNTs in water expanded up to ∼16000 times compared to its initial bed volume. Figure S3 presents various stages of MWNT expansion during sonication.

The unattached or residual TiO_2 was quantified by UV−vis absorption following a reported procedure[48] (Figure S4). The method's detection limit for TiO_2 was 0.4 μg/mL. The input concentrations of TiO_2 in our studied systems were 940−260 μg/mL. Therefore, the method was capable of detecting down to <1% residual/unattached TiO_2 in all experiments.

2.4. Characterization of MWNTs, TiO_2, and MWNT-TiO_2. The microstructure, morphology, surface area, pore size distribution, thermal stability, surface charge, aggregation, and polydispersity (in water) of the MWNTs, TiO_2, and MWNT-TiO_2 composite were characterized. Also, the MWNT-TiO_2 composite was tested for structural stability by dispersing in various organic solvents and in water at different pH values.

SEM. The microstructures of MWNTs, TiO_2, and MWNT-TiO_2 composite were examined by SEM using an FEI Helios

DOI: 10.1021/acsomega.8b02706
ACS Omega 2019, 4, 535−545

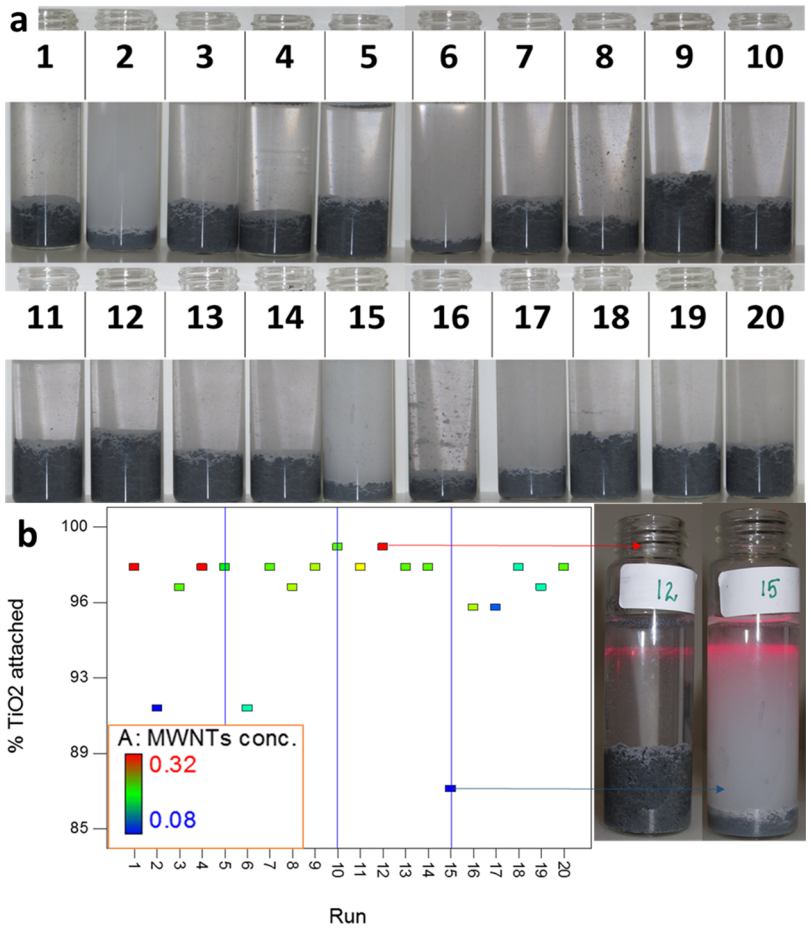

Figure 1. (a) Immobilization of TiO_2 on MWNTs to form MWNT-TiO_2 composite with numbers corresponding to experimental combinations proposed by CCD in Table 2. (b) Attachment of TiO_2 on MWNTs at different parameter combinations. Tyndall effect (right) qualitatively exhibits the presence of unattached TiO_2 particles.

from FEI Co. (Hillsboro, OR, USA) operating at 5 keV. The sample surface was coated with a 10 nm layer of gold and palladium using a GATAN Model 682 PECS before imaging.

Surface Area and Pore Size Distribution. BET surface area and porosity were measured by a NOVA 2200e automated gas sorption system (Quantachrome, FL, USA) using nitrogen gas at 77 K. The adsorption/desorption isotherms were measured at a relative pressure (P/P_0) ranging from 0.0001 to 0.99. The BET equation was used to determine the specific surface area.

TGA. Thermal analysis was carried out using a PerkinElmer thermogravimetric analyzer (Waltham, MA, USA) using nitrogen as a carrier gas. The temperature was gradually increased from 30 to 800 °C using approximately 10 mg of sample.

ζ-Potential. The surface charges on MWNTs, TiO_2, and MWNT-TiO_2 were measured in water using a ZetaPALS analyzer (Brookhaven, NY, USA). The Smoluchowski equation was used to calculate ζ-potentials from electrophoretic mobilities.[49] The details of ζ-potential measurements can be found elsewhere.[50]

Aggregation in Water. The aggregate sizes of MWNTs, TiO_2, and MWNT-TiO_2 in water were measured at 23 ± 1 °C using the ZetaPALS analyzer (Brookhaven, NY, USA). DLS was used to estimate the diameter of aggregates. The DLS (and ζ-potential) measurements were performed by varying pH and conductivity of the background solution using HCl, NaOH, phosphate buffer, and NaCl. Prior to particulate size measurements, the MWNTs were suspended in water with the aid of ultrasonication. A bath sonicator was used for ultrasonication together with an established protocol[51] to obtain stable suspensions.

Stability of MWNT-TiO_2 Composite. Interparticle interactions between MWNTs and TiO_2, responsible for the structural integrity of the MWNT-TiO_2 composite, were evaluated by dispersing the composite in various solvents and pH solutions. The mass percent of TiO_2 leaving the composite was quantified to estimate the disintegration of the composite. A series of solvents with various polarities, ranging from 0.1 (hexane) to 10.2 (water) on the polarity index,[52] were selected to assess hydrophobic interactions. Meanwhile, the electrostatic interactions were evaluated by testing the TiO_2 dislodging at pH 3 through pH 10.5.

3. RESULTS AND DISCUSSION

3.1. Evaluation of Design Parameters. The 20 MWNT-TiO_2 composite experimental preparation runs using different conditions (Figure 1a) demonstrated varying degrees of TiO_2 attachment as a function of MWNT concentration (Figure 1b). The Tyndall effect[53] of residual TiO_2 at the highest and the lowest MWNT concentrations was clearly observable between runs 12 and 15, respectively (Figure 1b). The Tyndall effect qualitatively describes the unattached TiO_2 in suspension.

The first step toward understanding the interactions between MWNTs and TiO_2 (to form MWNT-TiO_2 composite) was to

DOI: 10.1021/acsomega.8b02706
ACS Omega 2019, 4, 535−545

evaluate the synthesis parameters with respect to their relationship with composite formation. For this purpose, correlations between TiO_2 attached and MWNT concentration (Figure S5), Sonication 1 (Figure S6), and Sonication 2 (Figure S7) were evaluated. Sonication 1 was primarily for MWNT expansion, and sonication 2 was intended for MWNTs and TiO_2 mixing to form MWNT-TiO_2 composite. From the values of regression coefficient and MWNT expansion trend (blue to red), it is concluded that Sonication 1 is the most influential parameter for MWNT-TiO_2 composite synthesis. A reasonable correlation (0.72) exists between Sonication 1 and percent TiO_2 attached to MWNTs. The attachment of TiO_2 to MWNTs is directly proportional to Sonication 1, which is correlated to MWNT expansion.

The sonication depends on several parameters, including time of sonication, the sonicator's amplitude of vibration, pulse on/off duration, temperature, pressure, the shape of the container, physical (heat capacity, viscosity, density, boiling point), and chemical (inter- and intramolecular binding) properties of the solvent.[54] Unfortunately, the existing literature mostly describes sonication in terms of only one parameter, that is, sonication time. This led us to perform a separate study where we calibrated the sonicator (for sonication energy) and established the relationship between the sonicator's parameters and delivered sonication energy. There, a calorimetric approach was applied to calculate, model, and optimize the sonication energy delivered by a sonicator to an aqueous system. The details of the procedure adopted for calibration and optimization of sonication energy can be found elsewhere.[55] Another problem encountered was to estimate the relationship between the sonication energy and the quality of MWNT dispersions in water. For this purpose, the MWNT aggregate size and its distribution were examined in relation to sonication energy in various sonication conditions. The parameters that best dispersed MWNTs were sonication time of 19−180 s, amplitude of vibration of 144 μm, pulse on time of 24 s, and pulse off time of 15 s for a 30 mL solution. The details of MWNT dispersions affected by sonication can be found elsewhere.[55]

3.2. Model Development and Fitting. A second-order polynomial equation was developed to fit the experimental data. The general equation can be written as

$$\text{response} = b_0 + b_1A + b_2B + b_3C + b_{12}AB + b_{13}AC + b_{23}BC + b_{11}A^2 + b_{22}B^2 + b_{33}C^2 \quad (1)$$

where b_0 is constant; b_1, b_2, and b_3 are linear coefficients; b_{12}, b_{13}, and b_{23} are cross-product coefficients; and b_{11}, b_{22}, and b_{33} are quadratic coefficients. Equations 2−5 are the semiempirical relationships obtained by fitting the experimental data to eq 1.

MWNT expansion

$$= 10.5 - 1.8\,A + 3.1\,B + 1.8\,C \quad (2)$$

$$= 5.9 - 25.6 \times \text{MWNT conc.} + 0.15 \times \text{Sonication 1} + 0.14 \times \text{Sonication 2} \quad (3)$$

%TiO_2 attached

$$= 97.6 + 0.2A + 2.7B + 1.1C - 1.6BC - 1.6B^2 \quad (4)$$

$$= 77 + 3.5 \times \text{MWNT conc.} + 0.6 \times \text{Sonication 1} + 0.3 \times \text{Sonication 2} - 0.01 \times \text{Sonication 1} \times \text{Sonication 2} - 0.004 \times (\text{Sonication 1})^2 \quad (5)$$

Equations 2 and 3 are developed for MWNT expansion, and eqs 4 and 5 are for TiO_2 attachment on MWNTs. The coded equations (eqs 2 and 4) are useful to compute the relative impact of factors on responses (see Section 2.2 for explanation of coding). Meanwhile, the equations with actual factors (eqs 3 and 5) are derived from coded equations by scaling the coefficients to accommodate the units and are used to predict the responses quantitatively (using the same units). The response for eqs 2 and 3 is MWNT expansion, and eqs 4 and 5 is percent TiO_2 attachment. Equations 2 and 3 consist of three statistically significant terms, indicating that individual effects of factors are sufficient to explain MWNT expansion in water (Table S1). Unlike MWNT expansion, eqs 4 and 5 have nine statistically significant terms, which exhibit the importance of combined impact of factors (BC) and quadratic effect of Sonication 1 (B), along with their individual contribution toward TiO_2 attachment to MWNTs.

To establish the model, the experimental data were plotted against the values predicted from models in eqs 3 and 5. The plots between experimental and predicted MWNT expansion and percent TiO_2 attachment (Figure 2a,b, respectively) both

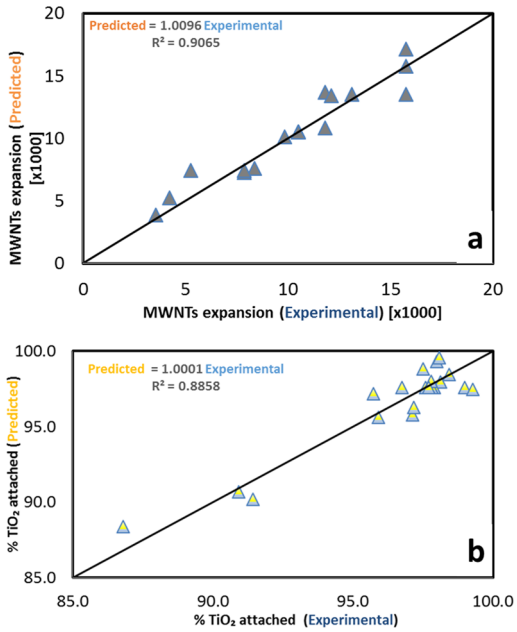

Figure 2. (a) Correlation between experimental and predicted values of MWNT expansion and (b) percent TiO_2 attached on MWNTs to make MWNT-TiO_2 composite. The experimental data occur on both sides of the predicted model response.

yielded a regression coefficient of ∼0.9, indicating a good correlation of experimental data with predicted values. Finally, the model was validated by performing ANOVA, which tests the significance and adequacy of the model.

3.3. Analysis and Diagnostics of the Model. Results were obtained from ANOVA of the model developed for MWNT exfoliation as represented by its volume expansion in water (eqs 2 and 3) (Table S1). The F-value of 49.52 implies the significance of the model. The p-values for the overall model and its three individual terms are below 0.0001, indicating their significance. The difference between predicted and adjusted R^2 is 0.06.Therefore, on the basis of ANOVA, the model is acceptable for prediction.

DOI: 10.1021/acsomega.8b02706
ACS Omega 2019, 4, 535−545

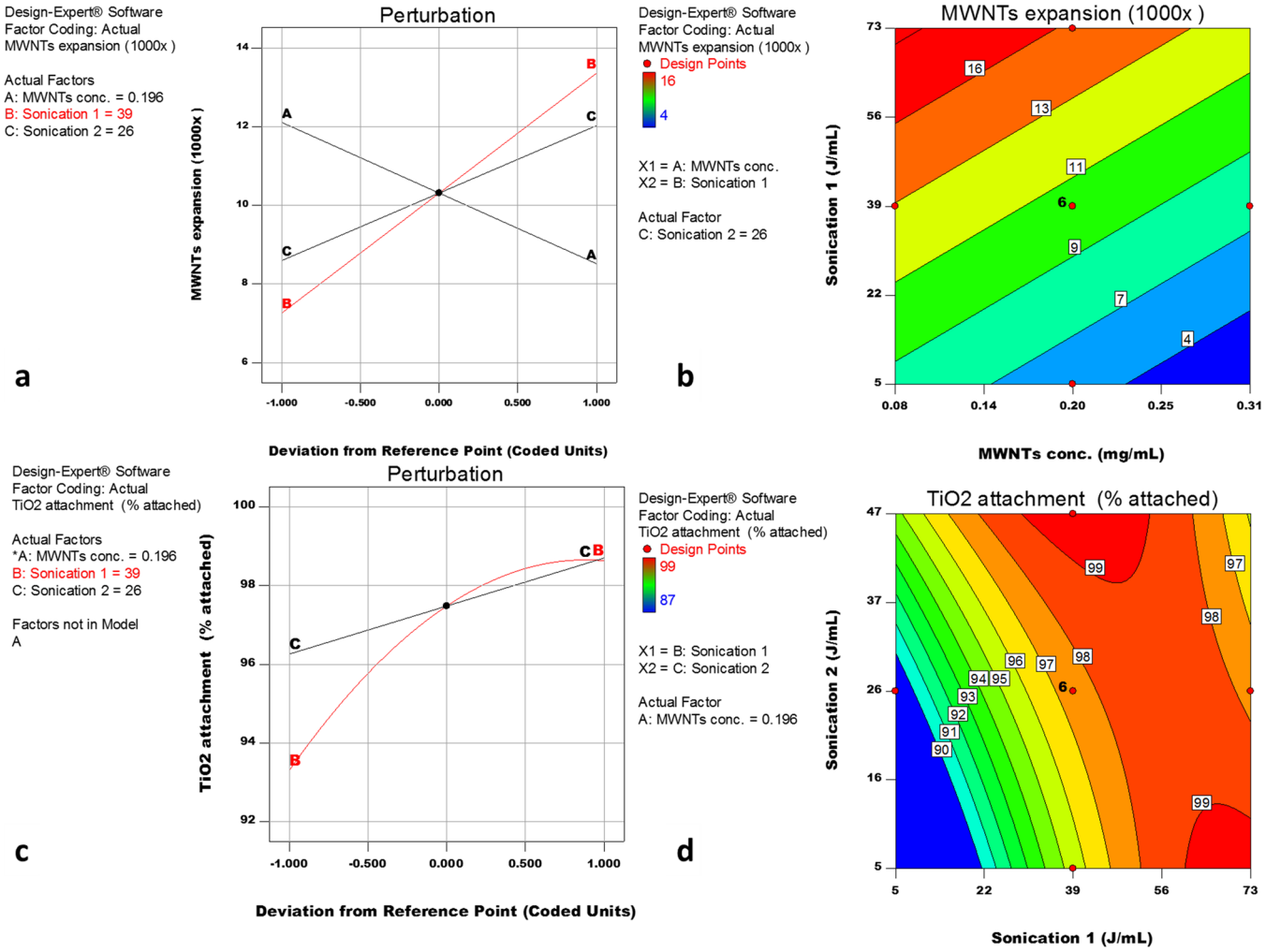

Figure 3. (a) Perturbation plot for MWNT expansion. Sonication 1 (*B*) and Sonication 2 (*C*) carry positive slopes, whereas MWNT conc. (*A*) has a negative slope, representing an increase in MWNT expansion with an increase of Sonication 1 and 2 and decrease of MWNT concentration. The *x*-axis of the perturbation plot is scaled according to coded values, and the inset shows the actual values of the intersection point, which is the center of the design space. (b) MWNT expansion as a function of the combined effect of Sonication 1 and MWNT concentration. (c) Perturbation plot for percent TiO_2 attachment. Sonication 1 (*B*) and Sonication 2 (*C*) carry positive slopes, indicating an increase in percent TiO_2 attachment with an increase of Sonication 1 and 2, where MWNT concentration is not playing any role (not shown). (d) Percent TiO_2 attachment as a function of the combined effect of Sonication 1 and Sonication 2. Red parabolic regions in the lower right corner and upper mid-right regions represent the highest (≥99%) TiO_2 attachment. Interestingly, TiO_2 attachment decreased upon increasing Sonication 2 beyond 25 J/mL. The concentration of MWNTs was kept at 0.2 mg/mL to obtain panel (d) as shown in the figure key along with the scale for percent TiO_2 attachment.

ANOVA results were obtained for the model developed to predict percent TiO_2 attached to MWNTs (eqs 4 and 5) (Table S2). The high *F*-value of 29.14 is indicative of model significance, that is, there is only 0.01% chance that this *F*-value is due to noise. The *p*-values for the model and all its terms (except MWNT conc.) are below 0.05; that is, they are significant. The difference between predicted and adjusted R^2 is below 0.2, showing their reasonable agreement. The ANOVA analysis, therefore, suggests the applicability of the model to predict TiO_2 attachment to MWNTs.

The model representing MWNT expansion (eq 2) carries three statistically significant terms. It shows that MWNT concentration, Sonication 1, and Sonication 2 all individually influence MWNT expansion. A perturbation plot was obtained by varying one factor at a time while keeping others constant (Figure 3a). The influence of each change on the response was monitored, and the slope of the plot indicated the influence cast by the selected factor. Plotting the factors together gives the relative impact of individual factors. The negative slope of *A* (MWNT conc.) represents the inversely proportional relationship between MWNT concentrations and MWNT expansion (Figure 3a). Similarly, the positive slope of *B* (Sonication 1) is indicative of an increase in MWNT expansion with the increase in Sonication 1. Factor *C* (Sonication 2) follows the same trend as *B*, but its slope is less steep than *B*, indicating its weaker positive contribution to MWNT expansion. The perturbation plot helped in identifying the important variables that were further diagnosed by plotting the contours corresponding to the 3D response surfaces. In the case of MWNT expansion, MWNT concentration and Sonication 1 are the most important variables. Therefore, we refit the data to examine the impact of just these two variables (Figure 3b). MWNT expansion is maximal at the lowest mass concentration and the highest Sonication 1 (red bands).

Unlike MWNT expansion, the TiO_2 attachment was more dependent on Sonication 2 than on MWNT concentration

DOI: 10.1021/acsomega.8b02706
ACS Omega 2019, 4, 535−545

(Figure 3c). The Sonication 1 parameter, however, remained the most influential factor. Another interesting observation was the curvature in the perturbation lines representing Sonication 1. The curvature exhibits a nonlinear response corresponding to the change in the value of a certain variable. Figure 3d is helpful in identifying the regions where maximum TiO_2 attachment can be obtained using the appropriate amount of Sonication 1 and Sonication 2.

Pareto analysis was performed to rank the effects of variables on responses. It provided the quantitative measure of the contribution of each significant model term (Figure 4). The

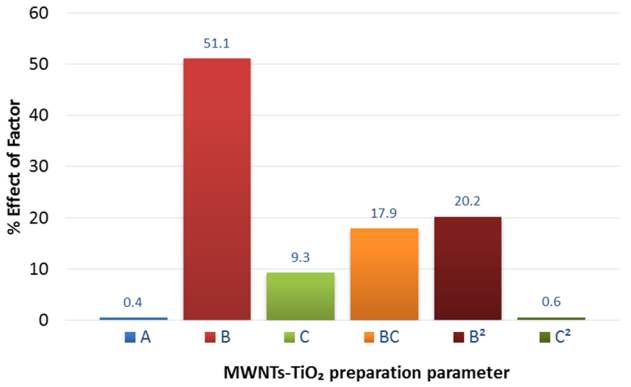

Figure 4. Pareto chart presenting percent contribution of MWNT concentration (A), Sonication 1 (B), and Sonication 2 (C) to percent TiO_2 attachment. BC represents the interaction contribution of Sonication 1 and Sonication 2. It can be inferred from the chart that the MWNT-TiO_2 synthesis mostly depends upon Sonication 1 (B, B^2, and BC).

Pareto analysis used the following equation to calculate the contribution of individual and interacting factors

$$P_n = 100 \times \left(\frac{b_n^2}{\sum b_n^2}\right) n \neq 0 \quad (6)$$

where P_n represents the percentage effect of each factor and b_n is the statistically significant coefficient of the polynomial equation (eq 1). In the case of MWNT expansion, eq 6 revealed that B (Sonication 1) contributes 60% to the process of expansion of MWNTs in water followed by A and C, each contributing 20% of the whole (not shown in Figure 4). In the case of TiO_2 attachment, Figure 4 shows that B (Sonication 1, individually) was responsible for more than half of the TiO_2 attachment followed by its self-interaction (B^2), interaction with Sonication 2 (BC), Sonication 2 (C), self-interaction of Sonication 2 (C^2), and MWNT concentration (A).

3.4. Optimization. Next, we used the results to optimize conditions for MWNT-TiO_2 composite synthesis (Table 3). The following question was addressed: "How can TiO_2 attachment be maximized in the presence of the highest concentration of MWNTs in water using the least amount of sonication energy?" The final goal (i.e., TiO_2 attachment) was assigned the maximum importance followed by its supportive response (MWNT bed expansion) while keeping MWNT concentration and Sonication 1 equally important. Sonication 2 exhibited a minimal impact from the diagnostics established, and therefore, it was assigned the minimum importance.

Table 3. Optimization Criteria for Synthesizing MWNT-TiO_2 Composite Using Sonication

constraints	goal	lower limit	upper limit	importance
A: MWNT conc.	maximize	0.13	0.27	2
B: Sonication 1	in range	18.8	59.2	2
C: Sonication 2	minimize	13.5	38.48	1
MWNT expansion	in range	4	16	3
% TiO_2 attached	maximize	87	99	5

The closeness of response toward the target, termed as desirability, can be mathematically defined as[56]

$$D = (d_1^{r1} \times d_1^{r2} \times d_1^{r3} \times \ldots \times d_1^{rn})^{1/\sum ri} \quad (7)$$

where n is the number of responses in the measure and r is the importance of responses from 1 (least important) to 5 (most important). The responses are multiplied; therefore, if even a single response reaches zero (falls outside their desirability range), the overall function becomes zero. Ramp function graphs with blue and red dots (Figure 5a) present three key factors and their two responses, respectively. The height of dot represents its desirability. A positive slope of the ramp represents the maximization of numerical value (MWNT conc. and Sonication 2) and vice versa (Sonication 2), defined in the optimization criteria. A flat ramp is indicative of uniform desirability as in the case of Sonication 1 and MWNT expansion. These two constraints are not specified under strict goals (i.e., maximize or minimize) for two reasons: (i) they are mutually inclusive, and (ii) manipulating them adversely affects desirability. Their effect on desirability is pronounced because of the extreme (5 out of 5) importance assignment to the ultimate goal, that is, percent TiO_2 attachment. Ramp graphs conclude the achievement of 97.4% of the set criterion (desirability achievement) when 0.26 mg/mL MWNTs were sonicated using 59.2 J/mL in the first stage (Sonication 1) and 13.5 J/mL in the second stage (Sonication 2). Also, this resulted in 9800 times expansion of MWNTs' original volume and attachment of 98.8% of the TiO_2 available in the aqueous system.

In the distribution of design space with respect to desirability (Figure 5b), the red region in the contour represents the design space, where over 90% desirability can be achieved. The "flag" in the right top corner of the red region represents the optimized point of achieving 97.4% desirability, previously discussed in the ramp plots (Figure 5a). This optimized point is very close to experimental run number 5 (factorial design point) in Table 2 (Materials and Methods).

In our final analysis, the effect of various factors on successful composite synthesis was studied. This exercise will be helpful to those who are interested in "responses" but do not generally agree with our defined desirability criteria, for instance, someone interested in only maximizing TiO_2 attachment irrespective of sonication energy expenditure (which we attempted to minimize for Sonication 2). The MWNT expansion and percent TiO_2 attachment were plotted against the most influential factors, MWNT concentration and Sonication 1 (Figure 5c,d, respectively). The top left corner of Figure 5c shows an orange region, which represents that an expansion of MWNTs over 14000 times can be achieved by lowering MWNT concentration down to 0.1 mg/mL and increasing Sonication 1 up to 60 J/mL. However, given the optimization criteria in Table 3, 9800 times expansion in MWNT initial volume serves the purpose of achieving the maximum (0.97) desirability. Similarly, a red region in Figure 5d is representative of the optimal zone, where maximum (≥98%) TiO_2 is attached to prepare the composite.

DOI: 10.1021/acsomega.8b02706
ACS Omega 2019, 4, 535−545

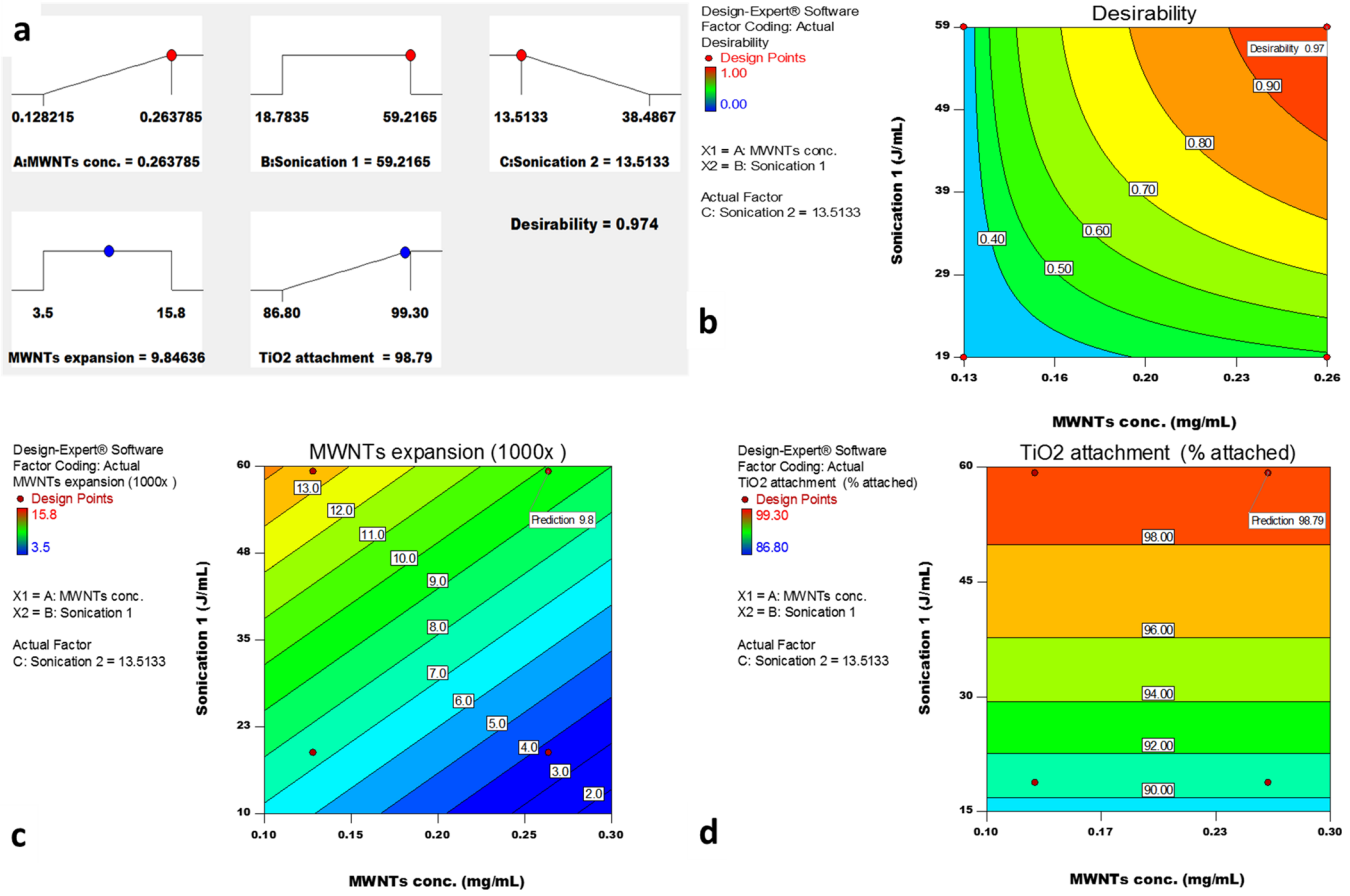

Figure 5. (a) Desirability ramps for optimization criteria described in Table 3. Ramps are a graphical representation of optimal solution. Flat ramps indicate uniform desirability (Sonication 1 and MWNT expansion), whereas inclined ramps represent minimum/maximum desired value. Red and blue dots represent factors and responses, respectively. The height of dot corresponds to the level of desirability achieved upon optimization. (b) Contour plot for desirability achievement according to the defined criteria. Contour plots for (c) MWNT expansion and (d) TiO_2 attachment with respect to Sonication 1 and MWNT concentration. The flags (inserted in b, c, and d) indicate specific points within the confines of the design and correspond to the optimum values shown in the ramps (a).

The flags are posted in Figure 5b–d to display our optimized design points.

3.5. Characterization of MWNTs, TiO_2, and MWNT-TiO_2. SEM micrographs were used to study the morphological structures of MWNTs, TiO_2, and MWNT-TiO_2 composite (Figure 6a,b and Figure S8). A close look reveals the wrapping of MWNTs over and around the TiO_2 particles. The diameter of MWNTs was ∼10 to 12 nm.

Nitrogen adsorption/desorption isotherms of MWNT-TiO_2 composite showed the MWNT-TiO_2 carried a specific surface area of 48.6 m^2/g (Figure 6c), which is lower than that of MWNTs (440.7 m^2/g) but higher than TiO_2 (15.6 m^2/g) (calculated from Figure S9). The weight ratio suggests the specific surface area of MWNT-TiO_2 composite to be 58.1 m^2/g, which is 17% more than the observed one (48.6 m^2/g). This decrease in surface area of the composite can be attributed to the decrease in nitrogen adsorption at interfaces of the two parent materials (MWNTs and TiO_2) as can be seen in the SEM micrographs (Figure 6a,b). The pore size distributions of MWNTs, TiO_2, and MWNT-TiO_2 composite indicate that the majority of the pores in MWNTs are mesopores, whereas TiO_2 carries micropores in excess (Figure 6d). The MWNT-TiO_2 composite inherits the porosity of both starting materials (Figure S10). There is evidence for the formation of some new pores in the MWNT-TiO_2 composite, which can be potential adsorption sites for appropriately sized molecules.

TGA of MWNTs, TiO_2, and MWNT-TiO_2 showed, contrary to expectations, the MWNT-TiO_2 composite was thermally more stable than its both parent materials (Figure 6e). The 10% MWNTs in the composite did not decompose throughout the studied range of temperature; instead, the mass of the composite kept on fluctuating above its original mass until 600 °C. It is hypothesized that TiO_2 entirely covered the MWNTs, leaving minimal free MWNTs. This can be seen in the SEM images (Figure 6a,b) as well. The fluctuation in the mass of composite might be due to the formation of functional groups at MWNT/TiO_2 junctions upon the increase in temperature because nitrogen and trace air were present in the atmosphere. It leads to the expectation of increased catalytic reactivity of MWNT-TiO_2 composite as compared to the TiO_2 alone.

The ζ-potential was indicative of ionically stabilized colloid systems (Figure 6f). They were mostly negative and are comparable to TiO_2 (see Figure S11). ANOVA revealed that except for pH 3.0 and 10.5, the ζ-potentials of TiO_2 and MWNT-TiO_2 are statistically indistinguishable from 0 at 95% confidence level. (The F-critical value was 4.5, where F-values for the measurements at pH 3, 4.5, 6, 7.5, 9, and 10.5 were 48.3, 3.4, 4.3, 0.44, 0.38, and 60.11.) This supports our hypothesis that the MWNTs were mostly surrounded by TiO_2 particles.

DOI: 10.1021/acsomega.8b02706
ACS Omega 2019, 4, 535−545

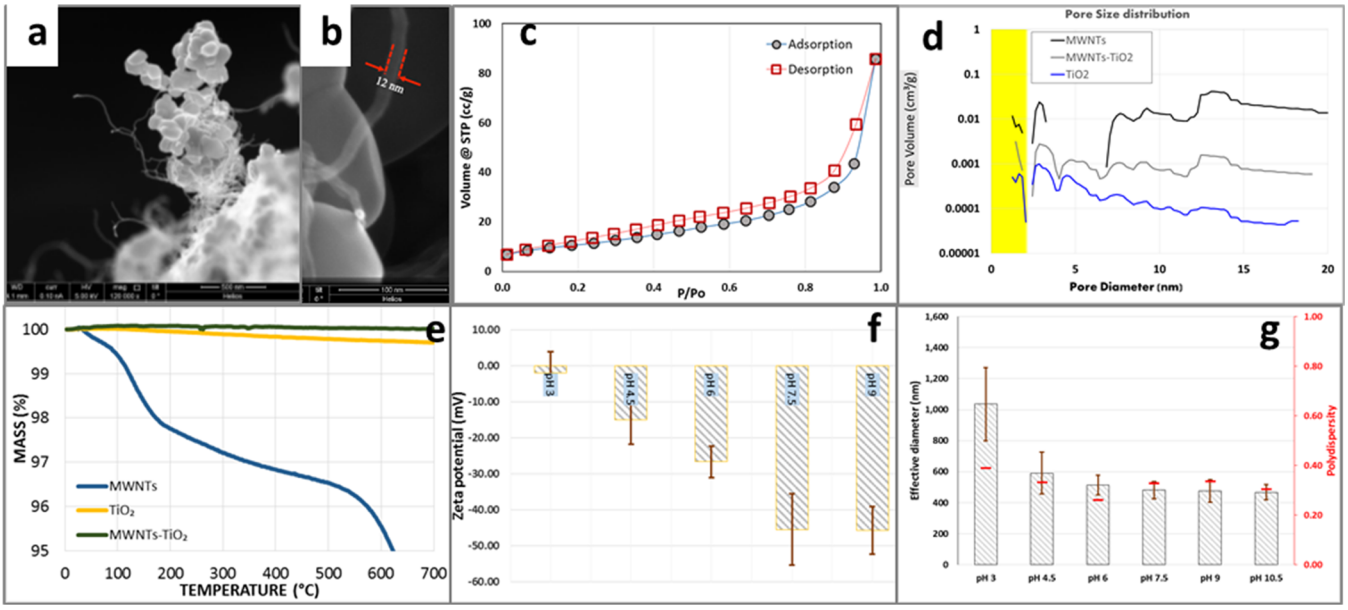

Figure 6. SEM of MWNT-TiO_2 at (a) 500 and (b) 100 nm magnification. The images reveal the clustering of TiO_2 around MWNTs having ~12 nm diameter. (c) Adsorption/desorption isotherm of nitrogen on MWNT-TiO_2 composite to calculate BET surface area estimated to be 48.6 m^2/g. (d) Pore size distributions of MWNT-TiO_2 and starting materials. MWNTs mostly contain mesopores, whereas TiO_2 contains micropores, resulting in the MWNT-TiO_2 to inherit the porosity of both materials, containing mesopores and micropores. (e) TGA of MWNT-TiO_2 and starting materials shows that MWNT-TiO_2 is the most thermally stable compound among the three. (f) ζ-potential of MWNT-TiO_2 was negative at the studied pH (3−9), which was similar to that of TiO_2. (g) Aggregation of MWNT-TiO_2 in water, at different pH, indicates that the composite's aggregate diameter was less than 1 μm. The polydispersity index values indicate that the MWNT-TiO_2 aggregates were fairly monodispersed at all studied pH (except pH 3 which seems closer to the isoelectric point of MWNT-TiO_2).

MWNT aggregation was mostly random, with a high polydispersity index, except at higher pH (Figure S12a). Meanwhile, TiO_2 particles were fairly monodispersed with small hydrodynamic radii (Figure S12b). The addition of MWNTs to TiO_2 (to form MWNT-TiO_2 composite) increased the average aggregate size of TiO_2 particles and slightly altered their polydispersity (Figure 6g).

Several factors can be responsible for holding MWNT and TiO_2 together in a composite (Figure S13a). Hydrophobic interactions were examined by observing the dispersion of MWNT-TiO_2 composites in a series of solvents with different polarities: hexane (0) < dichloromethane (3.1) < isopropanol (3.9) < acetone (5.1) < acetonitrile (5.8) < water (9) showed the TiO_2 leaving the composite was always below our method detection limit of 0.9 mg/L (corresponding to 0.04% mass of the initially attached TiO_2). The electrostatic interactions were tested by changing the pH of the background aqueous solution from pH 3 to 10.5 (Figure S13b). A maximum of 1.6% TiO_2 was observed to leave the composite at pH 10.5. Therefore, it can be assumed that hydrophobic and electrostatic interactions were not the significant attraction forces between MWNT and TiO_2 in a MWNT-TiO_2 composite. Hence, the composite can withstand extreme pH and polar/nonpolar background solvents without significantly disintegrating into its constituents.

4. CONCLUSIONS

The following conclusions were derived from this study:

1. The MWNT-TiO_2 composite can be prepared in a single pot following four steps: (i) addition of MWNTs to water, (ii) sonication to exfoliate MWNTs, (iii) addition of TiO_2, and (iv) sonication to mix and attach TiO_2 to MWNTs.
2. MWNT exfoliation (proportional to its bed volume expansion) by sonication is the most important parameter responsible for attachment of TiO_2 to MWNTs for MWNT-TiO_2 composite synthesis.
3. MWNT bed volume in water can be expanded up to ~16000 times by providing only 59 J/mL sonication energy in water under specific conditions (MWNT conc. = 0.13 mg/mL, vibration amplitude = 144 μm, and pulse on/off cycle = 24/15 s).
4. Over 99% of TiO_2 attachment to MWNTs can be achieved by optimizing MWNT concentration and sonication.
5. RSM is a powerful technique to obtain the optimum experimental design for MWNT-TiO_2 composite synthesis and optimization.
    i. A polynomial equation (model) was fitted to describe factors affecting MWNT-TiO_2 composite synthesis.
    ii. The model was tested statistically and experimentally.
    iii. The significant terms in models were analyzed, and their impact on responses was monitored.
    iv. The optimum MWNT-TiO_2 synthesis conditions, to maximize yield using minimal resources, were identified.
6. Characterization using SEM, TGA, ζ-potential analysis/DLS technique indicated the MWNTs being completely surrounded by TiO_2 particles in a MWNT-TiO_2 composite. The surface area and porosity analysis provided evidence for the attachment of TiO_2 on MWNTs through 17% reduction in overall surface area while mostly conserving the porosity of the parent materials. The stability of MWNT-TiO_2 composite, in

DOI: 10.1021/acsomega.8b02706
ACS Omega 2019, 4, 535−545

various solvents and at different pH, establishes reasonably strong interactions between MWNT and TiO_2 to hold the constituents together in a composite.

■ ASSOCIATED CONTENT

Supporting Information

The Supporting Information is available free of charge on the ACS Publications website at DOI: 10.1021/acsomega.8b02706.

ANOVA results for the response surface quadratic model of MWNT expansion and percent TiO_2 attached to MWNTs; photographic images presenting film formation ability of 100% TiO_2, MWNTs:TiO_2 (0.01:0.99), MWNT:TiO_2 (0.1:0.9), MWNT:TiO_2 (0.3:0.7), MWNT:TiO_2 (0.5:0.5), and 100% MWNTs on glass substrate; CCD presenting experimental points in the design space; expansion of MWNTs upon sonication; UV−vis 380 nm absorption of TiO_2 suspensions in water; correlation between MWNT concentration in water and percent TiO_2 attached, between sonication 1 (performed to exfoliate MWNTs) and percent TiO_2 attached, and between sonication 2 (performed to mix exfoliated MWNTs and TiO_2) and percent TiO_2 attached; SEM of MWNT-TiO_2 at different magnifications; nitrogen adsorption/desorption isotherms at 77 K, pore size distribution, ζ-potentials, effective diameter, and polydispersity of MWNTs, TiO_2, and MWNT-TiO_2; images of MWNT-TiO_2 composite dispersed in a series of solvents with different polarities and dispersed in a series of different pH solutions; plots showing polarities and corresponding dielectric constants of the solvents used and the mass percent of TiO_2 leaving the composite at different pH (PDF)

■ AUTHOR INFORMATION

Corresponding Author

*E-mail: farrukh.ahmad@ku.ac.ae. Phone: +971 (02) 8109114.

ORCID

Qammer Zaib: 0000-0002-1924-4131

Mustapha Jouiad: 0000-0002-7587-1500

Farrukh Ahmad: 0000-0003-1405-220X

Present Address

[‖]LPMC - EA2081, University of Picardie Jules Verne, Amiens, France

Funding

Masdar Institute of Science and Technology (grant no. SG2015-000029).

Notes

The authors declare no competing financial interest.

■ ACKNOWLEDGMENTS

We gratefully acknowledge the valuable feedback from Dr. Philip M. Gschwend of the Massachusetts Institute of Technology during the course of this study.

■ REFERENCES

(1) Bickley, R. I.; Gonzalez-Carreno, T.; Lees, J. S.; Palmisano, L.; Tilley, R. J. A structural investigation of titanium dioxide photocatalysts. *J. Solid State Chem.* **1991**, *92*, 178−190.

(2) Hurum, D. C.; Agrios, A. G.; Crist, S. E.; Gray, K. A.; Rajh, T.; Thurnauer, M. C. Probing reaction mechanisms in mixed phase TiO 2 by EPR. *J. Electron Spectrosc. Relat. Phenom.* **2006**, *150*, 155−163.

(3) Hurum, D. C.; Gray, K. A.; Rajh, T.; Thurnauer, M. C. Recombination pathways in the Degussa P25 formulation of TiO_2: surface versus lattice mechanisms. *J. Phys. Chem. B* **2005**, *109*, 977−980.

(4) Hurum, D. C.; Agrios, A. G.; Gray, K. A.; Rajh, T.; Thurnauer, M. C. Explaining the enhanced photocatalytic activity of Degussa P25 mixed-phase TiO_2 using EPR. *J. Phys. Chem. B* **2003**, *107*, 4545−4549.

(5) Kamat, P. V. Photoinduced transformations in semiconductormetal nanocomposite assemblies. *Pure Appl. Chem.* **2002**, *74*, 1693−1706.

(6) Yao, Y.; Li, G.; Ciston, S.; Lueptow, R. M.; Gray, K. A. Photoreactive TiO_2/carbon nanotube composites: synthesis and reactivity. *Environ. Sci. Technol.* **2008**, *42*, 4952−4957.

(7) Li, G.; Gray, K. A. The solid−solid interface: explaining the high and unique photocatalytic reactivity of TiO 2-based nanocomposite materials. *Chem. Phys.* **2007**, *339*, 173−187.

(8) Rajeshwar, K.; de Tacconi, N. R.; Chenthamarakshan, C. R. Semiconductor-based composite materials: preparation, properties, and performance. *Chem. Mater.* **2001**, *13*, 2765−2782.

(9) Chen, Y.; Dionysiou, D. D. A comparative study on physicochemical properties and photocatalytic behavior of macroporous TiO2-P25 composite films and macroporous TiO_2 films coated on stainless steel substrate. *Appl. Catal., A* **2007**, *317*, 129−137.

(10) Yoo, K. S.; Choi, H.; Dionysiou, D. D. Synthesis of anatase nanostructured TiO_2 particles at low temperature using ionic liquid for photocatalysis. *Catal. Commun.* **2005**, *6*, 259−262.

(11) Hwang, K.-J.; Lee, J.-W.; Shim, W.-G.; Jang, H. D.; Lee, S.-I.; Yoo, S.-J. Adsorption and photocatalysis of nanocrystalline TiO2 particles prepared by sol−gel method for methylene blue degradation. *Adv. Powder Technol.* **2012**, *23*, 414−418.

(12) Chen, Y.; Crittenden, J. C.; Hackney, S.; Sutter, L.; Hand, D. W. Preparation of a novel TiO_2-based p-n junction nanotube photocatalyst. *Environ. Sci. Technol.* **2005**, *39*, 1201−1208.

(13) Herrmann, J.-M. Heterogeneous photocatalysis: state of the art and present applications In honor of Pr. RL Burwell Jr.(1912−2003), Former Head of Ipatieff Laboratories, Northwestern University, Evanston (Ill). *Top. Catal.* **2005**, *34*, 49−65.

(14) Karkmaz, M.; Puzenat, E.; Guillard, C.; Herrmann, J. M. Photocatalytic degradation of the alimentary azo dye amaranth: Mineralization of the azo group to nitrogen. *Appl. Catal., B* **2004**, *51*, 183−194.

(15) Staniszewska, M.; Graca, B.; Nehring, I. The fate of bisphenol A, 4-tert-octylphenol and 4-nonylphenol leached from plastic debris into marine water − experimental studies on biodegradation and sorption on suspended particulate matter and nano-TiO_2. *Chemosphere* **2016**, *145*, 535−542.

(16) Daneshvar, N.; Salari, D.; Khataee, A. R. Photocatalytic degradation of azo dye acid red 14 in water on ZnO as an alternative catalyst to TiO_2. *J. Photochem. Photobiol., A* **2004**, *162*, 317−322.

(17) Khataee, A. R.; Fathinia, M.; Aber, S.; Zarei, M. Optimization of photocatalytic treatment of dye solution on supported TiO_2 nanoparticles by central composite design: Intermediates identification. *J. Hazard. Mater.* **2010**, *181*, 886−897.

(18) Falck, G. C.; Lindberg, H. K.; Suhonen, S.; Vippola, M.; Vanhala, E.; Catalan, J.; Savolainen, K.; Norppa, H. Genotoxic effects of nanosized and fine TiO_2. *Hum. Exp. Toxicol.* **2009**, *28*, 339−352.

(19) Dong, H.; Zeng, G.; Tang, L.; Fan, C.; Zhang, C.; He, X.; He, Y. An overview on limitations of TiO_2-based particles for photocatalytic degradation of organic pollutants and the corresponding countermeasures. *Water Res.* **2015**, *79*, 128−146.

(20) Carpio, E.; Zuniga, P.; Ponce, S.; Solis, J.; Rodriguez, J.; Estrada, W. Photocatalytic degradation of phenol using TiO 2 nanocrystals supported on activated carbon. *J. Mol. Catal. A: Chem.* **2005**, *228*, 293−298.

(21) Ohno, T.; Sarukawa, K.; Matsumura, M. Crystal faces of rutile and anatase TiO_2 particles and their roles in photocatalytic reactions. *New J. Chem.* **2002**, *26*, 1167−1170.

(22) Luttrell, T.; Halpegamage, S.; Tao, J.; Kramer, A.; Sutter, E.; Batzill, M. Why is anatase a better photocatalyst than rutile? - Model studies on epitaxial TiO_2 films. *Sci. Rep.* **2014**, *4*, 4043.

(23) Yao, Y. *Photoreactive Nano-composite for Membrane Filtration: Titanium Dioxide/Carbon Nanotube Composite for Photoreactive Membrane Filtration*. VDM Verlag Dr. Müller: Riga, Latvia, 2009.
(24) Raj, K. J. A.; Viswanathan, B. Effect of surface area, pore volume and particle size of P25 titania on the phase transformation of anatase to rutile. *Indian J. Chem., Sect. A: Inorg., Bio-inorg., Phys., Theor. Anal. Chem.* **2009**, *48*, 1378−1382.
(25) Bansal, R. C.; Goyal, M., *Activated Carbon Adsorption*. CRC Press: Boca Raton, FL, 2005.
(26) Puma, G. L.; Bono, A.; Krishnaiah, D.; Collin, J. G. Preparation of titanium dioxide photocatalyst loaded onto activated carbon support using chemical vapor deposition: A review paper. *J. Hazard. Mater.* **2008**, *157*, 209−219.
(27) Zhang, X.; Zhou, M.; Lei, L. Preparation of photocatalytic TiO_2 coatings of nanosized particles on activated carbon by AP-MOCVD. *Carbon* **2005**, *43*, 1700−1708.
(28) Araña, J.; Dona-Rodrıguez, J. M.; Rendón, E. T.; i Cabo, C. G.; González-Dıaz, O.; Herrera-Melián, J. A.; Pérez-Peña, J.; Colón, G.; Navıo, J. A. TiO_2 activation by using activated carbon as a support: Part II. Photoreactivity and FTIR study. *Appl. Catal., B* **2003**, *44*, 153−160.
(29) Yuan, R.; Zheng, J.; Guan, R.; Zhao, Y. Surface characteristics and photocatalytic activity of TiO 2 loaded on activated carbon fibers. *Colloids Surf., A* **2005**, *254*, 131−136.
(30) Wang, W.; Silva, C. G.; Faria, J. L. Photocatalytic degradation of Chromotrope 2R using nanocrystalline TiO 2/activated-carbon composite catalysts. *Appl. Catal., B.* **2007**, *70*, 470−478.
(31) Xu, Y.-J.; Zhuang, Y.; Fu, X. New insight for enhanced photocatalytic activity of TiO_2 by doping carbon nanotubes: a case study on degradation of benzene and methyl orange. *J. Phys. Chem. C* **2010**, *114*, 2669−2676.
(32) Woan, K.; Pyrgiotakis, G.; Sigmund, W. Photocatalytic carbon-nanotube-TiO_2 composites. *Adv. Mater.* **2009**, *21*, 2233−2239.
(33) Kang, S. Z.; Cui, Z.; Mu, J. Composite of Carboxyl-Modified Multi-walled Carbon Nanotubes and TiO_2 Nanoparticles: Preparation and Photocatalytic Activity. *Fullerenes, Nanotubes, Carbon Nanostruct.* **2007**, *15*, 81−88.
(34) Fan, W.; Gao, L.; Sun, J. Anatase TiO_2-Coated Multi-Wall Carbon Nanotubes with the Vapor Phase Method. *J. Am. Ceram. Soc.* **2006**, *89*, 731−733.
(35) Yu, Y.; Yu, J. C.; Chan, C.-Y.; Che, Y.-K.; Zhao, J.-C.; Ding, L.; Ge, W.-K.; Wong, P.-K. Enhancement of adsorption and photocatalytic activity of TiO 2 by using carbon nanotubes for the treatment of azo dye. *Appl. Catal., B* **2005**, *61*, 1−11.
(36) Feng, W.; Feng, Y.; Wu, Z.; Fujii, A.; Ozaki, M.; Yoshino, K. Optical and electrical characterizations of nanocomposite film of titania adsorbed onto oxidized multiwalled carbon nanotubes. *J. Phys.: Condens. Matter* **2005**, *17*, 4361.
(37) Jitianu, A.; Cacciaguerra, T.; Benoit, R.; Delpeux, S.; Beguin, F.; Bonnamy, S. Synthesis and characterization of carbon nanotubes−TiO2 nanocomposites. *Carbon* **2004**, *42*, 1147−1151.
(38) Thostenson, E. T.; Ren, Z.; Chou, T.-W. Advances in the science and technology of carbon nanotubes and their composites: a review. *Compos. Sci. Technol.* **2001**, *61*, 1899−1912.
(39) Kwak, J.-S. Application of Taguchi and response surface methodologies for geometric error in surface grinding process. *Int. J. Mach. Tools Manuf.* **2005**, *45*, 327−334.
(40) Bezerra, M. A.; Santelli, R. E.; Oliveira, E. P.; Villar, L. S.; Escaleira, L. A. Response surface methodology (RSM) as a tool for optimization in analytical chemistry. *Talanta* **2008**, *76*, 965−977.
(41) Gunaraj, V.; Murugan, N. Application of response surface methodology for predicting weld bead quality in submerged arc welding of pipes. *J. Mater. Process. Technol.* **1999**, *88*, 266−275.
(42) Khataee, A. Application of central composite design for the optimization of photo-destruction of a textile dye using UV/S2O82- process. *Polish J. Chem. Technol.* **2009**, *11*, 38−45.
(43) Box, G. E. P.; Hunter, J. S. The 2^{k-p} Fractional Factorial Designs Part I. *Technometrics* **1961**, *3*, 311−351.
(44) Box, G. E. P.; Hunter, J. S. Multi-factor experimental designs for exploring response surfaces. *Ann. Math. Stat.* **1957**, *28*, 195−241.
(45) Obeng, D. P.; Morrell, S.; Napier-Munn, T. J. Application of central composite rotatable design to modelling the effect of some operating variables on the performance of the three-product cyclone. *Int. J. Miner. Process.* **2005**, *76*, 181−192.
(46) Napier-Munn, T. J. *The Central Composite Rotatable Design*; JKMRC, The University of Queensland: Brisbane, Australia, 2000; pp 1−9.
(47) Sakkas, V. A.; Islam, M. A.; Stalikas, C.; Albanis, T. A. Photocatalytic degradation using design of experiments: a review and example of the Congo red degradation. *J. Hazard. Mater.* **2010**, *175*, 33−44.
(48) Dietrich, L. A. S.; Sahu, M.; Biswas, P.; Fein, J. B. Experimental study of TiO 2 nanoparticle adhesion to silica and Fe (III) oxide-coated silica surfaces. *Chem. Geol.* **2012**, *332*, 148−156.
(49) Zaib, Q.; Khan, I. A.; Saleh, N. B.; Flora, J. R. V.; Park, Y.-G.; Yoon, Y. Removal of Bisphenol A and 17β-Estradiol by Single-Walled Carbon Nanotubes in Aqueous Solution: Adsorption and Molecular Modeling. *Water, Air, Soil Pollut.* **2012**, *223*, 3281−3293.
(50) Zaib, Q.; Mansoor, B.; Ahmad, F. Photo-regenerable multi-walled carbon nanotube membranes for the removal of pharmaceutical micropollutants from water. *Environ. Sci.: Processes Impacts* **2013**, *15*, 1582−1589.
(51) Zaib, Q.; Khan, I. A.; Yoon, Y.; Flora, J. R. V.; Park, Y. G.; Saleh, N. B. Ultrasonication study for suspending single-walled carbon nanotubes in water. *J Nanosci. Nanotechnol.* **2012**, *12*, 3909−3917.
(52) Skoog, D. A.; Holler, F. J.; Crouch, S. R. *Principles of Instrumental Analysis*. Thomson Brooks/Cole: Pacific Grove, CA, 2007.
(53) Li, D.; Müller, M. B.; Gilje, S.; Kaner, R. B.; Wallace, G. G. Processable aqueous dispersions of graphene nanosheets. *Nat. Nanotechnol.* **2008**, *3*, 101−105.
(54) Santos, H. M.; Lodeiro, C.; Capelo-Martínez, J.-L. The Power of Ultrasound. In *Ultrasound in Chemistry: Analytical Applications*; Wiley-VCH Verlag GmbH & Co. KGaA: Berlin, 2009; pp 1−16.
(55) Zaib, Q. *Multiwalled carbon nanotubes / Titanium dioxide for water treatment: Synthesis, characterization, and application*. Masdar Institute of Science and Technology, Khalifa University: Abu Dhabi, UAE, 2016.
(56) Anderson, M. J.; Whitcomb, P. J. *RSM Simplified: Optimizing Processes Using Response Surface Methods for Design of Experiments*. Productivity Press: New York, 2005.

DOI: 10.1021/acsomega.8b02706
ACS Omega 2019, 4, 535−545